Bayesian moment tensor inversion and uncertainty quantification for induced seismicity – uncertainties from both the location and velocity model

Chen Gu, Youssef M. Marzouk and M. Nafi Toksöz, Massachusetts Institute of Technology*

Summary

In many oil/gas fields and hydrofracking processes induced earthquakes result from fluid extraction or injection. The locations and source mechanisms of these earthquakes provide valuable information about the reservoirs. Analysis of induced seismic events has mostly assumed a double-couple source mechanism. However, recent studies have shown a non-negligible percentage of non-double-couple components of source moment tensors in hydraulic fracturing events. Without uncertainty quantification of the moment tensor solution, it is difficult to determine the reliability of these source models. This study develops a Bayesian method to perform waveform-based full moment tensor inversion and uncertainty quantification for the induced seismic events. We conduct tests with synthetic events to validate the method, and then apply our Bayesian inversion approach to real induced seismicity events.

Introduction

Induced micro-earthquakes happen widely in conventional and unconventional oil/gas fields. Induced seismicity study is of great importance in monitoring and understanding the processes of hydraulic fracturing, fluid injection and oil/gas extraction (Maxwell et al., 2014; Shapiro, 2015). Source mechanism inversion is one of the main areas of the induced seismicity studies. The determination of source mechanisms of induced earthquakes can give the stress and fault orientation in the field (Vavryčuk, 2014).

Many studies have implemented the inversion of the full moment tensor by the least-squares (LSQ) method and the regularized LSQ method (Sipkin, 1982; Šílený, 1992, 1996). However, LSQ methods have disadvantages in estimating and interpreting the uncertainty of the moment tensor solutions, since the LSQ methods only search for the best moment tensor solution and do not naturally yield probability distributions on the solution. An important question for full moment tensor inversion is whether the non-DC components are real. Some research has applied an *F*-test to check the significance of the non-DC components (Templeton, 2006, Šílený, 2009, Horalek, 2010, Nayak, 2014). LSQ methods do allow a limited uncertainty quantification, based on the Hessian of the misfit function near the LSQ point estimate. But this is only a local and linearized estimate of uncertainty, and can be difficult to interpret. Alternatively, to address the uncertainties of moment tensors resulting from the data noise or imperfect station coverage, many LSQ-based moment tensor inversion studies have applied resampling methods to the data, such as Monte Carlo noise realization methods and jackknife tests (Šílený, 2009; Stierle, 2014a,b).

Compared to LSQ methods, Bayesian inversion methods naturally quantify the uncertainty in model parameters by characterizing a posterior probability distribution over the parameter space (Tarantola, 2005; Kaipio, 2006; Stuart 2010). Some studies have conducted Bayesian moment tensor inversion for moderate and large earthquakes. Duputel (2012) introduced a Bayesian moment tensor inversion method to estimate the uncertainties of source mechanisms for large earthquakes ($M_w \geq 6.0$) from a global seismic network. That study did not determine the uncertainty of seismic locations jointly with the moment tensor. Stähler et al. (2014, 2016) presented a detailed study of probabilistic moment tensor and depth inversion from P and S-waveforms, as well as error modeling and station covariances during seismic source inversion. A recent paper by Mustać 2016, has developed a Bayesian full moment tensor inversion for a moderate-size earthquake with a well-studied source mechanism using a regional seismic network. In that research, the uncertainties of both the seismic location and the moment tensor have been studied by implementing an outer Markov chain to sample the location parameters, and an inner chain to sample the moment tensor parameters.

In this study, we introduce a waveform-based Bayesian full moment tensor inversion method with the consideration of uncertainties from both the location and velocity model. Both the uncertainties of seismic moment tensor and location are analyzed. Unlike the Bayesian method implemented by Mustać (2016), we sample the source location, velocity model and the moment tensor parameters using a single Markov chain; this approach reduces computational cost and provides more accurate uncertainty estimates, particularly for the source location. Moreover, we use the conditionally Gaussian structure of the parameter posterior to solve portions of the inverse problem analytically, reducing the dimension of the sampling problem and allowing the impact of source location uncertainty on moment tensor uncertainty to be explicitly quantified. We first validate the method using synthetic data before applying this full moment tensor inversion method to a selected induced event in an oil/gas field in Oman (Figure 1). The seismicity of this field and source mechanisms of events using DC assumptions have been studied extensively (Sarkar, 2008; Li et al., 2011a, b). To better quantify the uncertainties, we use the newly developed waveform-based Bayesian method for full moment tensor inversion and uncertainty quantification.

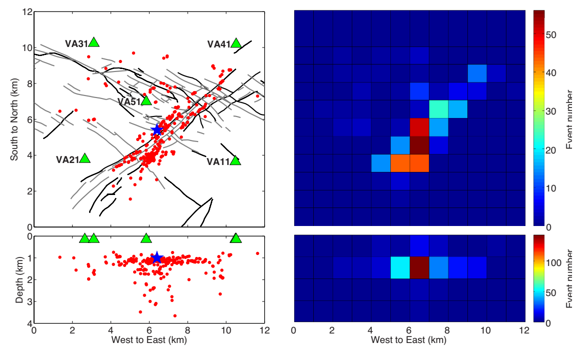

Figure 1: Left: Map view and side view of the stations and located events for the near-surface network (Sarkar 2008; Li et al., 2011a, b). The red dots denote the location of the detected events, and the green triangles show the location of the stations. The black lines are the identified faults. The green triangles (VA11, VA21, VA31, VA41, and VA51) are the five near-surface stations. These stations are located in shallow boreholes 150 m below the surface. Right: Map view and side view of the spatial distribution of the microseismic events on the left. Our synthetic and selected real data are from one of the densest blocks along the fault.

Bayesian Inversion Method and Synthetic Tests

Before the Bayesian inversion, we first construct a Green's function library, and calculate the synthetic seismograms for a point moment tensor source using the discrete wavenumber integration method (Bouchon, 1981). The observed seismogram v_i^n of the ith component at the nth geophone of location x_r^n is modeled by

$$\boldsymbol{w}_i^n(\boldsymbol{x}_r^n, \boldsymbol{x}_s, t) = \sum_{j=1}^{3}\sum_{k=1}^{3} \boldsymbol{M}_{jk}\boldsymbol{G}_{ij,k}(\boldsymbol{x}_r^n, \boldsymbol{x}_s, \boldsymbol{v}, t) * s(t) + \boldsymbol{e}_i^n(t) \qquad (1)$$

where $\boldsymbol{G}_{ij,k}(\boldsymbol{x}_r^n, \boldsymbol{x}_s, t)$ is the spatial derivative of the Green's function at the nth geophone of the location $\boldsymbol{x}_r^n$ due to a point moment tensor source of the location $\boldsymbol{x}_s, \boldsymbol{v}$ is the 1-D velocity model, $s(t)$ is the source time function and $e_i^n(t)$ is the noise perturbation of ith component at the nth geophone. Since $\boldsymbol{M}_{jk}$ is a symmetric matrix, we can simplify m_{jk} to a vector m of six elementary moment tensor parameters, i.e., $m_1 = M_{11}, m_2 = M_{22}, m_3 = M_{33}, m_4 = M_{12}, m_5 = M_{12}$, $m_6 = M_{23}$. Then Equation 1 is written as

$$\boldsymbol{d} = \boldsymbol{G}(\boldsymbol{x}, \boldsymbol{v})\boldsymbol{m} + \boldsymbol{e} \qquad (2)$$

where $\boldsymbol{x}$ denotes the source location $\boldsymbol{x}_s$ in Equation 1, $\boldsymbol{d}$ is the catenation of all the waveform vector $\boldsymbol{w}_i^n$, $\boldsymbol{G}(\boldsymbol{x})$ is the catenation of all the synthetic seismograms of six elementary moment tensor parameters, and $\boldsymbol{e}$ is the catenation of all the noise vectors. The objective of the Bayesian inversion is to predict parameters $\boldsymbol{m}$ and $\boldsymbol{x}$ in Equation 1 and quantify their uncertainties based on the waveform $\boldsymbol{d}$.

We apply the Bayesian rule to the parameter $\boldsymbol{m}$ and $\boldsymbol{x}$ given waveform data $\boldsymbol{d}$

$$P(\boldsymbol{m}, \boldsymbol{x}, \boldsymbol{v}|\boldsymbol{d}) = \frac{P(d|\boldsymbol{m}, \boldsymbol{x}, \boldsymbol{v})\pi_0(\boldsymbol{m})\pi_0(\boldsymbol{x})\pi_0(\boldsymbol{v})}{P(\boldsymbol{d})} \qquad (3)$$

where $\pi_0(\boldsymbol{m})$ and $\pi_0(\boldsymbol{x})$ are the prior probability density functions of $\boldsymbol{m}$ and $\boldsymbol{x}$, $P\,(d|\boldsymbol{m}, \boldsymbol{x}, \boldsymbol{v})$ is the likelihood function, $P(\boldsymbol{d})$ is the evidence (or marginal likelihood), and $P(\boldsymbol{m}, \boldsymbol{x}, \boldsymbol{v}|\boldsymbol{d})$ is the posterior probability density function.

We assume the uniform distribution assumptions for $\pi_0(\boldsymbol{m})$ and $\pi_0(\boldsymbol{x})$, and the Gaussian noise assumption for the data noise $\boldsymbol{e}$

$$\boldsymbol{e} \sim \boldsymbol{N}(0, \boldsymbol{\Sigma_e}), \qquad (4)$$

where $\boldsymbol{\Sigma_e}$ is the block-diagonal matrix with the noise variance of a particular component of seismograms $(\sigma_i^n)^2$ as the diagonal elements of the block related to that seismic component. The likelihood function can be presented as

$$P(d|\boldsymbol{m}, \boldsymbol{x}, \boldsymbol{v}) = \frac{1}{\sqrt{(2\pi)^N|\Sigma_e|}} \exp\left[-\frac{1}{2}(\boldsymbol{d} - \boldsymbol{G}(\boldsymbol{x}, \boldsymbol{v})\boldsymbol{m})^T\boldsymbol{\Sigma_e^{-1}}(\boldsymbol{d} - \boldsymbol{G}(\boldsymbol{x}, \boldsymbol{v})\boldsymbol{m})\right] \qquad (5)$$

where N is the total number of data samples used for inversion. With the prior and likelihood functions, we can obtain the joint posterior distribution of $\boldsymbol{M}$ and $\boldsymbol{x}$

$$P(\boldsymbol{m}, \boldsymbol{x}, \boldsymbol{v}|\boldsymbol{d}) = \frac{c}{\sqrt{(2\pi)^N|\Sigma_e|}} \exp\left[-\frac{1}{2}(\boldsymbol{d} - \boldsymbol{G}(\boldsymbol{x}, \boldsymbol{v})\boldsymbol{m})^T\boldsymbol{\Sigma_e^{-1}}(\boldsymbol{d} - \boldsymbol{G}(\boldsymbol{x}, \boldsymbol{v})\boldsymbol{m})\right] \qquad (6)$$

where c is a normalization constant.

The general method for posterior sampling $\boldsymbol{m}$, $\boldsymbol{x}$ and $\boldsymbol{v}$ is the Markov Chain Monte Carlo (MCMC) sampling method. The Metropolis-Hasting algorithm (Metropolis et al. 1953; Hastings 1970) is used to update the model parameters through the MCMC chain. Although we have the joint posterior function of $\boldsymbol{m}$, $\boldsymbol{x}$, and $\boldsymbol{v}$ - $P(\boldsymbol{m}, \boldsymbol{x}, \boldsymbol{v}|\boldsymbol{d})$ - based on Equation 6, the linear dependence on $\boldsymbol{m}$ and nonlinear dependence on $\boldsymbol{x}$ and $\boldsymbol{v}$ of the modeling waveforms $\boldsymbol{G}(\boldsymbol{x}, \boldsymbol{v})$ result in a complex joint dependence of $P(\boldsymbol{m}, \boldsymbol{x}, \boldsymbol{v}|\boldsymbol{d})$ on $\boldsymbol{m}$, $\boldsymbol{x}$, and $\boldsymbol{v}$. We can hardly sample $\boldsymbol{m}$, $\boldsymbol{x}$ and $\boldsymbol{v}$ simultaneously. We try the following approach to solve this problem.

We construct three MCMC chains for $\boldsymbol{m}$, $\boldsymbol{x}$, and $\boldsymbol{v}$. We first sample both $\boldsymbol{x}$, and $\boldsymbol{v}$ based the marginal posterior probability distribution $P(\boldsymbol{x}, \boldsymbol{v}|\boldsymbol{d})$, which can be analytically obtained by the integral of Equation (6) for all the $\boldsymbol{m}$. For the MCMC chain for $\boldsymbol{v}$, each $\boldsymbol{v}$ is proposed uniformly from a pool of velocity models. In this paper, we generate thousands of velocity models by the random Gaussian perturbation of the initial velocity model from well logs. For the MCMC chain for $\boldsymbol{x}$, each $\boldsymbol{x}$ is proposed by a random walk from the previous step. An adaptive metropolis (**AM**) Markov Chain Monte Carlo (MCMC) method (Haario et al. 2001) is used. The **AM** scheme adjusts the covariance matrix of $\boldsymbol{x}$ every n_0 steps through the MCMC chain based on all the previous samples of $\boldsymbol{x}$

$$\boldsymbol{C}_{n_0} = s_{dim}\boldsymbol{Cov}(x_0, \dots, x_{n_0}) + \epsilon_0 \boldsymbol{I}_{dim} \quad (10)$$

where $\boldsymbol{C}_{n_0}$ is the updated covariance matrix at step n_0, $\epsilon_0 > 0$ which is a constant to make $\boldsymbol{C}_{n_0}$ positive-definite, $dim = 3$ for $\boldsymbol{x}$, and $s_{dim} = 2.42/dim$. For the MCMC chain of $\boldsymbol{m}$, we implement the Gibbs sampling based on marginal-then-conditional $P(\boldsymbol{m}|\boldsymbol{d}, \boldsymbol{x}^*, \boldsymbol{v}^*)$ where $\boldsymbol{x}^*$ and $\boldsymbol{v}^*$ are given.

$$P(\boldsymbol{m}|\boldsymbol{d}, \boldsymbol{x}^*, \boldsymbol{v}^*) \sim \boldsymbol{N}\big(\boldsymbol{\mu_m}(\boldsymbol{d}, \boldsymbol{x}^*, \boldsymbol{v}^*), \boldsymbol{\Sigma_m}(\boldsymbol{d}, \boldsymbol{x}^*, \boldsymbol{v}^*)\big), \quad (7)$$

$$\boldsymbol{\mu_m}(\boldsymbol{d}, \boldsymbol{x}^*, \boldsymbol{v}^*) = [\boldsymbol{G^T}(\boldsymbol{x}^*, \boldsymbol{v}^*)\boldsymbol{G}(\boldsymbol{x}^*, \boldsymbol{v}^*)]^{-1}\boldsymbol{G^T}(\boldsymbol{x}^*, \boldsymbol{v}^*)\boldsymbol{d}, \quad (8)$$

$$\boldsymbol{\Sigma_m}(\boldsymbol{d}, \boldsymbol{x}^*, \boldsymbol{v}^*) = [\boldsymbol{\Sigma_m^0} + \boldsymbol{G^T}(\boldsymbol{x}^*, \boldsymbol{v}^*)\boldsymbol{\Sigma_e}\boldsymbol{G}(\boldsymbol{x}^*, \boldsymbol{v}^*)]^{-1}, \quad (9)$$

where $\boldsymbol{\Sigma_M^0}$ is the covariance matrix of M from the prior information of $\boldsymbol{m}$. The three MCMC chains are serially catenated, which means for each MCMC step we Gibbs update $\boldsymbol{m}$ first, and then update $\boldsymbol{x}$ and $\boldsymbol{v}$. The uncertainties of $\boldsymbol{m}$, $\boldsymbol{x}$, and $\boldsymbol{v}$ are quantified by the mean and covariance of posterior sampling from the three MCMC chains.

To validate our method, we first applied our full waveform inversion method to the synthetic data. The configuration of the seismic source and stations was shown in Figure 2. The synthetic source is located at $\boldsymbol{x} =$ [6.4, 5.4, 1.0] km. The source mechanism was set Strike = 50°, Dip = 40°, Rake = 280°, DC% = 61%, CLVD% = 17%, ISO = 21%, α = 10°, k = 1.0 ($k = \lambda/\mu$ where λ and μ are Lamé parameters). A layer velocity model was used in the synthetic tests (Figure 2, lower right). A 10% Gaussian noise was added to the synthetic data.

We first generate 1000 velocity models by 1% Gaussian perturbation of the initial velocity model. We show the log marginal posterior probability distribution $\log P(\boldsymbol{x^i}, \boldsymbol{v^j}|\boldsymbol{d})$ in Figure 3a), where $\boldsymbol{i}$ (=1, 2, …, 27) and $\boldsymbol{j}$ (=1, 2, …, 1000) are indexes for location and velocity in their corresponding pools, where the location and velocity are proposed. The MCMC chains for moment tensor, location, and velocity are shown in Figure 3b)-d). Note that to show the upper bounds of the uncertainties here, we assume the noise standard deviation to be 100% the maximum amplitude of each waveform. However, Even with this high noise assumption, the moment tensor, location, and velocity parameters are well recovered by this method.

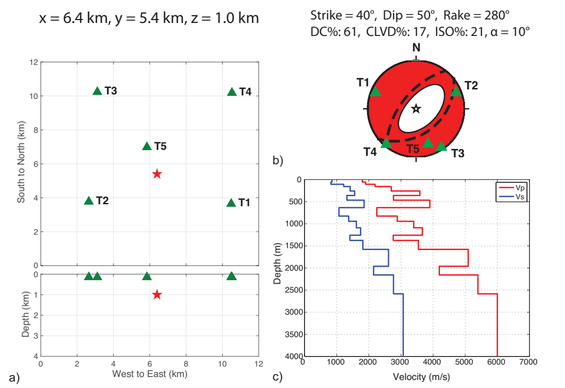

Figure 2: The configuration of source and stations of our synthetic data. Left: The locations of the source and the stations. The red star denotes the source, the green triangles denote the stations. We use the red lines to mark stations with the same x, y coordinates. Right: The beach ball on the top right shows the mechanism of the synthetic source. The green triangles denote the projection of the 5 stations on the source focal plane and the black dashed curve shows the projection of fault planes. The velocity model is shown at the bottom right.

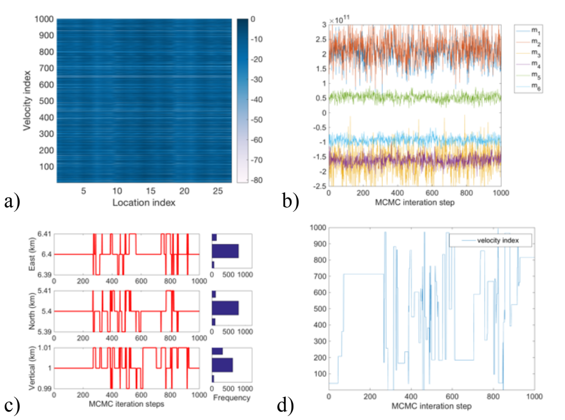

Figure 3: a): The normalized analytically-obtained log marginal lilelyhood $P(\boldsymbol{x^i}, \boldsymbol{v^j}|\boldsymbol{d})$; b): The MCMC chain for six moment tensor parameters; c) The MCMC chain for three location parameters and their probability distributon; d) The MCMC chain for velocity model index $\boldsymbol{j}$.

Results for real data

The field seismicity data are from the surface monitoring networks (Figure 1) in an oil and gas field in Oman. For the surface monitoring network, five surface stations, instrumented with SM-6B geophones, have been set up since 1999. The data used in the studies consist of 800 events located by the surface. This field is dominated by two fault systems – the northeast-southwest trending main faults and northwest-southeast trending auxiliary system.

We selected 1 event with high signal noise ratio from the surface monitoring network. The Bayesian inferred source mechanism and location with the uncertainties are shown in Figure 4. For this real data, we only implement the Bayesian inversion of moment tensor inversion with the consideration for location. However, based on the synthetic tests. We expect that the inclusion of velocity model uncertainties broadens the uncertainties of the both moment tensor and location solutions and provide more realistic uncertainty bounds.

Conclusion

The Bayesian moment tensor inversion method works well for recovering the source mechanisms and location from the seismograms; this is validated by our synthetic study. Running a single Markov chain with our marginal-then-conditional sampling approach significantly reduced the dimension of the sampling problem and its computational costs. In addition, the Bayesian method naturally lets us extract the uncertainties of the source parameters and location from the posterior distributions of these parameters.

Based on the synthetic simulation and the study of an induced seismic event, we can state that the uncertainty quantification of full moment tensor solutions is a powerful tool to estimate how reliable the source mechanism model is.

This study also includes the uncertainty of the velocity model. The inclusion of velocity model uncertainties broadens the uncertainties of the both moment tensor and location solutions and provide more realistic uncertainty bounds.

Acknowledgement

We thank Petroleum Development Oman (PDO) for providing field data. We acknowledge the Kuwait Foundation for the Advancement of Sciences and the Kuwait-MIT Center for Natural Resources and the Environment for their support during this work.

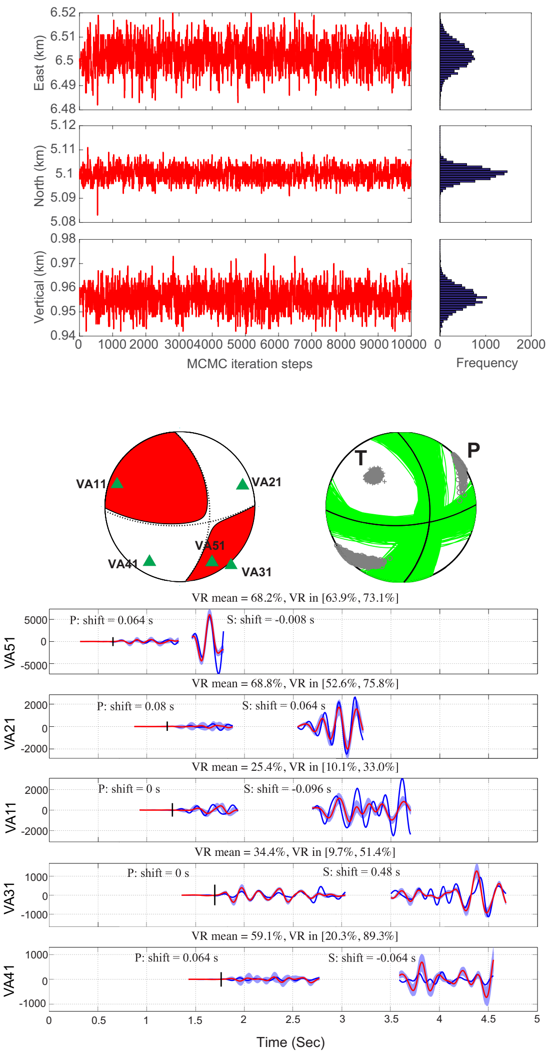

Figure 4: Top: The MCMC chanins for $\boldsymbol{x}$ and the resultant probability distribution for $\boldsymbol{x}$. Bottom: The focal plane projection of the source mechanism. The dashed line shows the mean value of the fault plane solutions. The green triangles denote the five stations. The green region shows the uncertainty of the fault plane solutions and the gray dots and crosses show the tensile and compressional stress from marginal-then-conditional sampling of m. The comparison of the mean posterior predicted (red) and real (blue) data for the separated P- and S-wave segments. The purple shading areas show the 10^4 posterior predicted waveforms. The mean and range of the variance reduction (VR) for each station is shown in the figure.